



The Use of Infrared Thermography on the Measurement of Microstructural Changes of Reservoir Rocks Induced by Temperature

Thomas Junique, Patricia Vázquez, Céline Thomachot-Schneider, Issra Hassoun, Mirlène Jean-Baptiste, Yves Géraud

► To cite this version:

Thomas Junique, Patricia Vázquez, Céline Thomachot-Schneider, Issra Hassoun, Mirlène Jean-Baptiste, et al.. The Use of Infrared Thermography on the Measurement of Microstructural Changes of Reservoir Rocks Induced by Temperature. Applied Sciences, 2021, 11 (2), pp.559. 10.3390/app11020559 . hal-03114708

HAL Id: hal-03114708

<https://hal.science/hal-03114708>

Submitted on 27 Aug 2021

HAL is a multi-disciplinary open access archive for the deposit and dissemination of scientific research documents, whether they are published or not. The documents may come from teaching and research institutions in France or abroad, or from public or private research centers.

L'archive ouverte pluridisciplinaire **HAL**, est destinée au dépôt et à la diffusion de documents scientifiques de niveau recherche, publiés ou non, émanant des établissements d'enseignement et de recherche français ou étrangers, des laboratoires publics ou privés.



Distributed under a Creative Commons Attribution 4.0 International License

Article

The Use of Infrared Thermography on the Measurement of Microstructural Changes of Reservoir Rocks Induced by Temperature

Thomas Junique ^{1,*} , Patricia Vazquez ¹ , Céline Thomachot-Schneider ¹ , Issra Hassoun ¹,
Mirlène Jean-Baptiste ¹ and Yves Géraud ²

¹ GEGENAA EA 3795, University of Reims Champagne-Ardenne 2, Esplanade Roland Garros, 51100 Reims, France; patricia.vazquez@univ-reims.fr (P.V.); celine.schneider@univ-reims.fr (C.T.-S.); issra.hassoun@etudiant.univ-reims.fr (I.H.); Mirlène.jean-baptiste@etudiant.univ-reims.fr (M.J.-B.)

² GeoRessources Laboratory UMR 7359, University of Lorraine, F54505 Vandoeuvre Les Nancy, France; yves.geraud@univ-lorraine.fr

* Correspondence: thomas.junique@univ-reims.fr

Abstract: A variation of temperature produces a change in the microstructure of the rock due to the mineral thermal expansion and its residual strain. Depending on the temperature cycle and texture, microstresses may lead to the development of preexistent cracks or the creation of a new and irreversible cracking. The effect of temperature on reservoir rocks is an important topic since it conditions the permeability and the fluid flow. Two main questions arise from this: the first is if an irreversible cracking threshold is attained in the reservoir rocks at low temperature geothermal systems (around 100 °C); the second one is about the influence of thermal fatigue by the repetition of heating–cooling cycles on the different rock types. To answer these questions, four reservoir rocks (chalk, sandstone, fresh granite, and weathered granite) were submitted to two different thermal regimes. The first test was conceived to detect the irreversible cracking threshold, and for that, the rocks were submitted to progressive heating (90°, 100°, 110°, 120°, and 130 °C). The second test consisted of doing cycles of fast heating of the samples up to 200 °C. The microstructure variation was assessed by means of a scanning electron microscope, mercury porosimetry, and capillary water uptake combined with passive infrared thermography. Infrared thermography is an emerging tool in the field of rock study, used to detect water masses or determine thermal properties. The water transfer during the capillary tests of the rocks, before and after the tests, was monitored with this technique. In addition, the cooling rate index, a non-destructive parameter to detect cracking development, was calculated. The results made it possible to differentiate the behaviours in relation to the rock type, with a chalk and a weathered granite less susceptible to thermal stresses than a fresh granite and sandstone. In addition, infrared thermography resulted in being a very useful indirect technique to detect the changes on the surface, although they do not always correlate to the bulk microstructural changes.

Keywords: infrared thermography; reservoir rocks; thermal fatigue; thermal threshold; microstructure



Citation: Junique, T.; Vazquez, P.; Thomachot-Schneider, C.; Hassoun, I.; Jean-Baptiste, M.; Géraud, Y. The Use of Infrared Thermography on the Measurement of Microstructural Changes of Reservoir Rocks Induced by Temperature. *Appl. Sci.* **2021**, *11*, 559. <https://doi.org/10.3390/app11020559>

Received: 8 December 2020

Accepted: 5 January 2021

Published: 8 January 2021

Publisher's Note: MDPI stays neutral with regard to jurisdictional claims in published maps and institutional affiliations.



Copyright: © 2021 by the authors. Licensee MDPI, Basel, Switzerland. This article is an open access article distributed under the terms and conditions of the Creative Commons Attribution (CC BY) license (<https://creativecommons.org/licenses/by/4.0/>).

1. Introduction

The influence of temperature on rock behaviour is studied in several geological domains, such as petroleum extraction, geothermal activity, or storage of radioactive waste, involving many rocks [1–4]. The research studies show that high temperature changes the minerals and the void system of the rocks and the flow of the fluid in the rock may be enhanced or reduced [5–9].

The intensity of the modifications of the porous network is related to inherent stone characteristics such as mineralogy, texture, weathering degree [10], and thermal regimes involving extreme temperatures and repetition cycles. Chalk, sandstone, and granite

are reservoir rocks, and their properties and behaviours facing different temperatures and pressure are often compared due to their different porous network, that is high microporosity for chalk, mesoporous distribution for sandstone, and low porosity of fissural type for granites.

Chalk is an interesting reservoir rock characterised by a large microporosity, with around 40% of void volume or even up to 50% for the North Sea Chalk [11]. The main features are its very rich to almost pure calcite composition and its reactivity to water. Despite the high and anisotropic thermal extension of calcite crystals, the high microporosity usually accommodates the expansion. Some authors show that heating, even at very high temperatures, does not modify the elastic parameters of the chalk but rather causes an extension of the elastic phase [3]. In the case of a fluid flow, chalk crystals are prone to dissolution or remobilisation, which creates a modification in chalk microstructure [12].

Sandstone (5–30%) is considered, due to its porosity, as a good reservoir rock and forms aquifers exploited as geothermal systems. The submission to high temperatures can trigger effects such as crushing of sand grains, fracturing, thermal expansion, or mineral cohesion rupture [13–15], generating changes in permeability [13,16,17].

Granite is very sensitive to the effects of temperature due to its low porosity (from around 1% to a few% if weathered) and its mineral heterogeneity and its differential thermal expansion [18–21]. That may lead to the generation of irreversible microcracks beyond a certain temperature threshold (e.g., [22–26]). In addition, for fresh and low porosity granites, textural features such as Quartz/Feldspar ratio, mineral orientation, or crystal size become determinants in its behaviour [21,27–29].

When a stone is exposed to high temperatures, two questions about its behaviour arise. Which is the threshold of irreversible cracking? Secondly, when the heating–cooling cycles are repeated, what is the effect of thermal fatigue on the stones? Thus, the main aim of this study is to assess the microstructural variation of four rocks analogous to those found in hydrocarbons reservoirs or as geothermal energy sources submitted to different thermal regimes. For that purpose, two kinds of tests were performed: Thermal Threshold (TT)—progressive heating cycles from 90 °C to 130 °C to determine the stone crack threshold, and Thermal Fatigue (TF)—thermal fatigue with cycles of heating–cooling at 200 °C.

The rock microstructure was evaluated before, during, and after the tests by several methods. A microscopical evaluation by scanning electronic microscopy was carried out to localise the new formed cracks. The variations of the bulk stone were carried out by mercury porosimetry. This technique gives information about the pore access distribution, which allows one to compare the size and frequency of the rock pore access ratio before and after heating [20,30–32].

To ensure the evolution continuity, capillary water uptake was also used to control the rock microstructure. This technique is non-destructive and allows one to quantify indirectly the microcrack formation or variation in the same sample through the cycles [33–35]. Capillary kinetics are related not only to porosity volume but also to pore width and connectivity, being complementary to mercury porosimetry.

New techniques are being developed for the study of rock state that can be applied in situ, such as infrared thermography (IRT). This technique measures the thermal response of the outer layers of the materials.

IRT allows one to visualise the fluid flow [36–39], and to quantify the thermal kinetics of the rocks. They are directly related to porosity [40–42] or decay state [43], and, consequently, a heated stone will reach the temperature equilibrium with the environment faster with higher porosity.

The natural cooling of a rock can be expressed by the cooling rate index (CRI) following the works of [44,45] that shows a direct correlation between the degree of fracturing and the cooling of the rock. Laboratory tests revealed a good correlation between the CRI during the first 10 min of cooling and the rock porosity, although for rocks with a porosity over 20% [41,42]. This technique allows one also to detect notable porosity variations

given by the thermal behaviour of the outer layers, which may reflect the changes in the bulk microstructure. In addition, there may be a contrast between internal and external thermal damage in sandstone for example. It has been established that thermal stresses distributed in rock can induce tensile stresses in a thin region near the outside, producing microcracking, and compressive stresses in a large area in the middle, producing healing or closing of microcracks [46].

A specific aim of this study is to test the cooling rate index quantified by infrared thermography as a technique to determine the microstructural state of the selected rocks from their behaviour on the outer layers. In addition, the capillary water uptake was monitored with this technique. The objective is to know if this non-destructive technique can be applied accurately in the case of rock thermal degradation in rocks with different porosity distribution.

2. Materials

Four types of rocks analogous to those used in the fields of storage, geothermal energy, and hydrocarbon systems were chosen for this study: a chalk, a sandstone, a fresh granite, and a weathered granite (Figure 1).

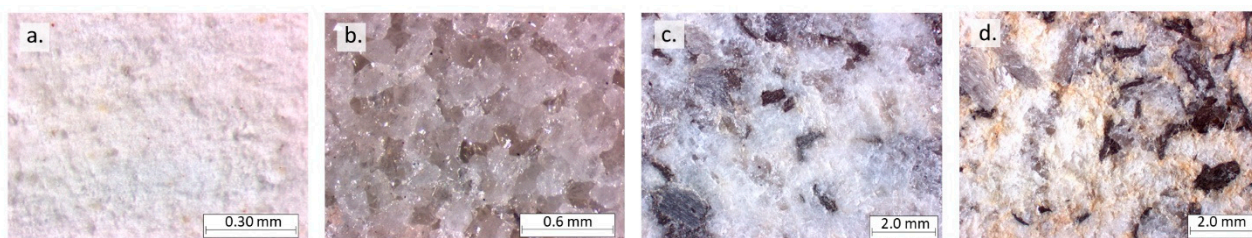


Figure 1. Selected rocks. Photographs made under a binocular microscope. (a) Châlons chalk (CC); (b) Fontainebleau sandstone (FS); (c) Gris Alba granite (GA); (d) Golden Ski granite (GS).

Châlons chalk (CC): The chalk dated from the Upper Cretaceous and belongs to the Paris basin structure (France). Samples were extracted from the Grand Mont quarry (Saint-Germain-la-Ville, France). From a mineralogical point of view, the Châlons chalk consisted almost exclusively of calcium carbonate ($\text{CaCO}_3 > 98.5\%$).

Fontainebleau Sandstone (FS): The sandstone is dated from the Lower Oligocene and belongs to the Paris basin structure (France). Samples were extracted from the Fontainebleau quarry, (Fontainebleau, France). This rock has the particularity of being composed almost exclusively of quartz (>99%) with constant grain size, with a median diameter of about 300 μm [47].

Gris Alba Monzogranite (GA): This rock belongs to the peraluminous syn and post-kinematic granites from the Galicia-tas-os-montes domain [48]. It is temporally related to regional metamorphism and processes of Hercynian crustal anatexis. The granitoid was quarried in the Salvaterra–A Cañiza–Cerdedo alignment belonging to the Faro de Avión batholith (Galice, Spain). The study revealed a homogeneous monzogranite with a fine grain (2–5 mm). Quartz and plagioclase appeared in a similar proportion (around 25%) while alkali feldspar showed a higher proportion with almost 40%. The proportion of muscovite:biotite minerals is about 2:1 [28].

Golden Ski Monzogranite (GS): Golden Ski is a peraluminous syn-kinematic granite that belongs also to the Galicia-Tras-os-montes Zone of the Iberian Massif. The samples were quarried close to the border between Galice (Spain) and Portugal. Similar to GA, this rock is located in the Salvaterra–A Cañiza–Cerdedo alignment. GS is a homogeneous monzogranite with a fine grain (2–4 mm). Quartz appeared in a proportion close to 50% of the stone, while alkali feldspar and plagioclase showed a similar quantity with around 20% each. Mica appeared similarly distributed, with 13% in total. Habits go from subhedral (feldspars) to euhedral (muscovite) with quartz showing irregular shape. This granite showed an initial alteration characterised by the presence of clay and yellow colour [28].

3. Methodology

3.1. Experimental Setup

The four stones were exposed to two different thermal tests: Thermal Threshold Test (TT) and Thermal Fatigue Test (TF).

















Thermal Threshold Test (TT): The first experiment aimed to determine if a crack threshold is produced for each rock at a geothermal low temperature. For this purpose, the samples were exposed to 5 cycles of progressive heating and cooling at 90 °C, 100 °C, 110 °C, 120 °C, and 130 °C. A climatic chamber “Vötsch VC3” was used to produce a low heating and cooling rate of 1 °C·min^{−1}. This value was assigned to ensure that induced microcracks were the direct response of temperature and not the temperature gradient within the sample [9,49–52]. The temperature was maintained for 2 h [30,53] and the cooling was also performed at a low rate (1 °C·min^{−1}) to avoid thermal shock.


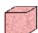
Thermal Fatigue Test (TF): The second experiment aimed at knowing the effect of thermal fatigue by temperature cycles. The samples went through 5 cycles of heating at 200 °C in a furnace “Thermo scientific led M 110” with a gradient of 5 °C·min^{−1} to ensure the cracking [16,54–57]. As in TT, the samples were maintained at the set temperature for 2 h and the cooling down was slow with a rate of about 0.5–1 °C·min^{−1}.

3.2. Analysis of the Variations

Samples of each stone type were submitted to each test, with different dimensions in relation to the analytical approach (Table 1): Scanning Electron Microscopy (SEM), mercury injection porosimetry (MIP), or capillary uptake + IRT. Two samples of size 10 mm × 40 mm × 40 mm corresponded to those tested continuously through every cycle for the capillary water uptake test (CWUT) and one of them was monitored by IRT. A total of 32 samples of size 10 mm × 10 mm × 15 mm were used for MIP destructive measurements, one sample per cycle and stone for TT and one sample per stone after cycle one and five (200(1) °C and 200(5) °C) for TF. SEM observations were undertaken before and after the experiments on 16 samples of 10 mm × 10 mm × 15 mm size: on each initial stone and after being tested at 130 °C, 200(1) °C and 200(5) °C.

Table 1. Specification of the measurement conditions for samples subjected to the two thermal treatments: Thermal Threshold test (TT) and Thermal Fatigue test (TF).

TT						TF					
Cycle	Temp.	CWUT	IRT	MIP	SEM	Cycle	Temp.	CWUT	IRT	MIP	SEM
0	Initial state					0	Initial state			-	-
1	90 °C	 ↓	 ↓		-	1	200(1) °C	 ↓	 ↓		
2	100 °C				-	2	200(2) °C			-	-
3	110 °C				-	3	200(3) °C			-	-
4	120 °C				-	4	200(4) °C			-	-
5	130 °C					5	200(5) °C				

 : 10 mm × 40 mm × 40 mm;  : 10 mm × 10 mm × 15 mm. Temp.: assigned temperature; CWUT: capillary water uptake tests; MIP: mercury injection porosimetry; SEM: scanning electron microscopy; IRT: infrared thermography.

3.2.1. Scanning Electron Microscopy (SEM)

SEM images for the studied rocks were taken and assessed with a SEM Hitachi TM-1000. The porous space was quantified in the initial state as well as at 130 °C and 200(1) °C.

3.2.2. Mercury Injection Porosimetry (MIP)

Mercury injection porosimetry (MIP) was determined with a Micromeritics AutoPore IV 950. The pressures applied were from 0 to 345 kPa measuring the pores of access radii ranging between 1.8 and 180 μm for the low-pressure stage, and up to 228 MPa for the quantification of pores between 0.003 and 3 μm .

3.2.3. Capillarity Water Uptake

The samples were dried at $40 \pm 5\text{ }^{\circ}\text{C}$ until constant weight before each test. Then, each sample was suspended from an electronic precision balance and put into contact with water in its bottom face at a depth of about 1 mm (Figure 2). The weight was automatically recorded every 10 s on a control computer. The test was carried out for 1 h, enough for all the samples to reach the stabilisation of the water uptake and the capillary coefficient (C) calculated from the obtained data. The temperature of the room was kept at $23 \pm 1\text{ }^{\circ}\text{C}$.

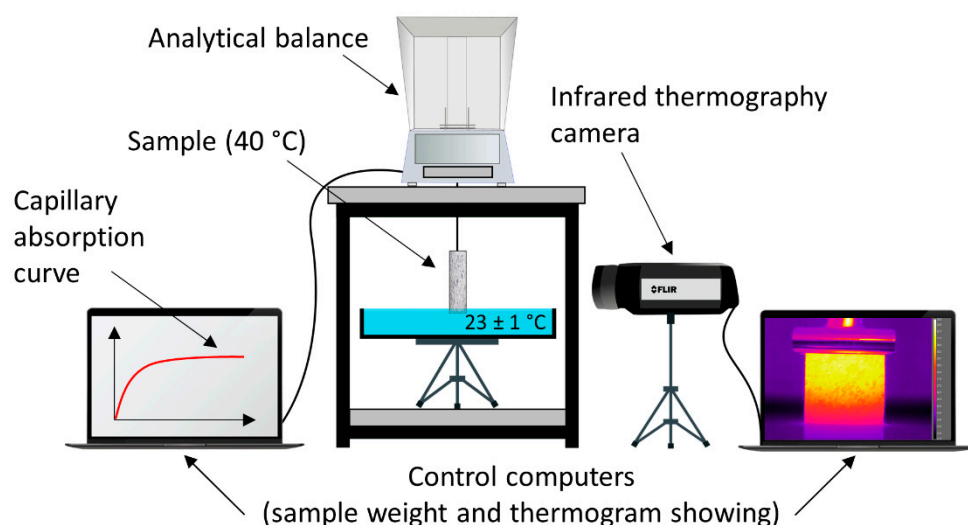


Figure 2. Experimental setup of capillary uptake controlled by automatic weight and IRT monitoring.

3.2.4. IRT Monitoring

One of the two tested samples was monitored with IRT during the capillary water uptake test, that is one sample by rock type and cycle. The complete setup is shown in Figure 2.

The monitoring was performed by a FLIR SC655 operating in wavelengths between 7.5 and 14 μm . The detection temperature of this device is between -40 and $150\text{ }^{\circ}\text{C}$ with a sensitivity of $0.1\text{ }^{\circ}\text{C}$. The detector is an uncooled array of microbolometers. The image size is 640×480 pixels and the noise signal is about 40 mK. The recorded signal is called thermosignal (TS) and it depends on temperature and emissivity, expressed in isothermal units (IUs).

The measurements were performed in passive IRT mode, that is, without any external heat source. The risks associated with environmental variations were minimised (control of temperature and humidity, room lights off). The IRT camera recorded thermal images at a rate of 6 frames/minute for 30 min. The recordings were processed by the FLIR ResearchIR software.

Two informations were obtained from the IRT data: the monitoring of the wet fringe along the samples and the rock cooling rate index (CRI 10, [44]), since the water rise did not reach the upper part of the samples during the first minutes, and the cooldown (from $40\text{ }^{\circ}\text{C}$ to $23\text{ }^{\circ}\text{C}$) was done by exchange with the room temperature (Figure 3a).

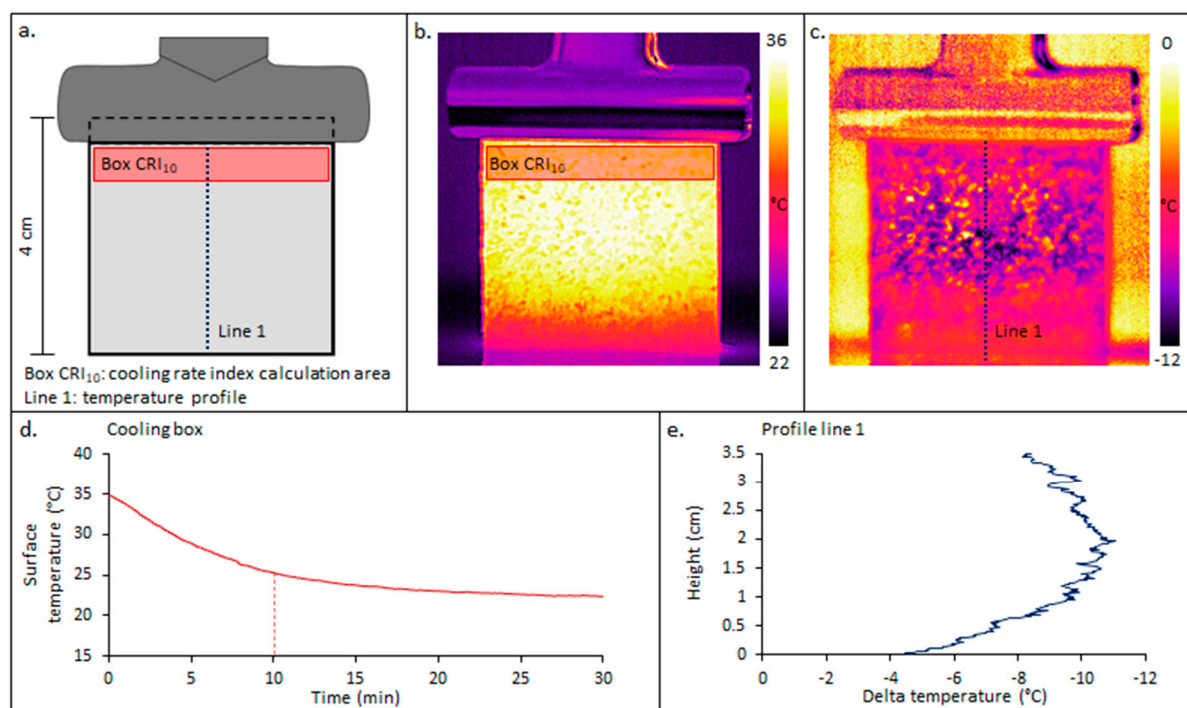


Figure 3. IRT setup. (a) Schema of the sample and the measurements carried out. (b) IRT image in false colour. (c) Image after the application of a subtraction and an Advanced Plateau Equalisation (APE) scale. (d) Cooling curves. (e) Interpretation of the IRT image.

Wet fringe migration

The obtained IRT image during capillary water uptake revealed clearly the water presence on the rock (Figure 3b). However, with the rock cooling, the wet fringe and the details of the image were less and less evident with time. For that reason, a subtraction filter was applied, which produced images as the difference between the initial state and during the capillary test. In addition, an Advanced Plateau Equalisation (APE) scale was selected since it allowed us to observe more details and contrast from the rock (Figure 3c). A profile in the middle of the sample was plotted at different times to observe the water migration (Figure 3e).

Cooling rate index (CRI)

From the upper part of the sample (Figure 3a,b), the “Temporal Plot” function of the software gives the thermosignal evolution with time. The calculation of CRI is as follows:

$$\text{CRI} = \frac{\Delta T}{\Delta t} = \frac{T_{10} - T_0}{t_{10} - t_0} \quad (1)$$

where T_{10} is the temperature after 10 min of cooling, T_0 the initial temperature, t_{10} and t_0 are, respectively, the times with a lapse of around 10 min. In the case of chalk, with a very fast water absorption kinetics, the CRI was calculated for the first five minutes, before the water reaches the upper half. The data used were the cooling slopes related to the square root of time. High slope values corresponded to fast cooling and low values to a slow cooling (Figure 3d).

4. Results

4.1. Scanning Electron Microscopy Observations

The porous network of the rocks before and after the main heating cycles viewed under SEM is shown in Figure 4.

The Châlons chalk showed a homogeneous microporous network. The main components of the rock are well-preserved coccolith fragments of different shapes, although the

majority are elliptical with no preferred orientation. The coccolith length distribution was unimodal with a median of 4.2 μm and an interquartile range of about 2 μm . The contacts between the coccolith fragments were mainly punctate as well as between the micrites. The porosity was mainly composed of an interparticle microporosity inside the nanofossil cells (diameter < 1 μm). A few pores of around several microns in diameter have been observed. During the TT and TF test, the microtexture shows little major modification. The chalk surface at 200(5) $^{\circ}\text{C}$ appeared more irregular than the fresh samples, showing more grains clustered together and pore regions with enlarged interparticle spaces.

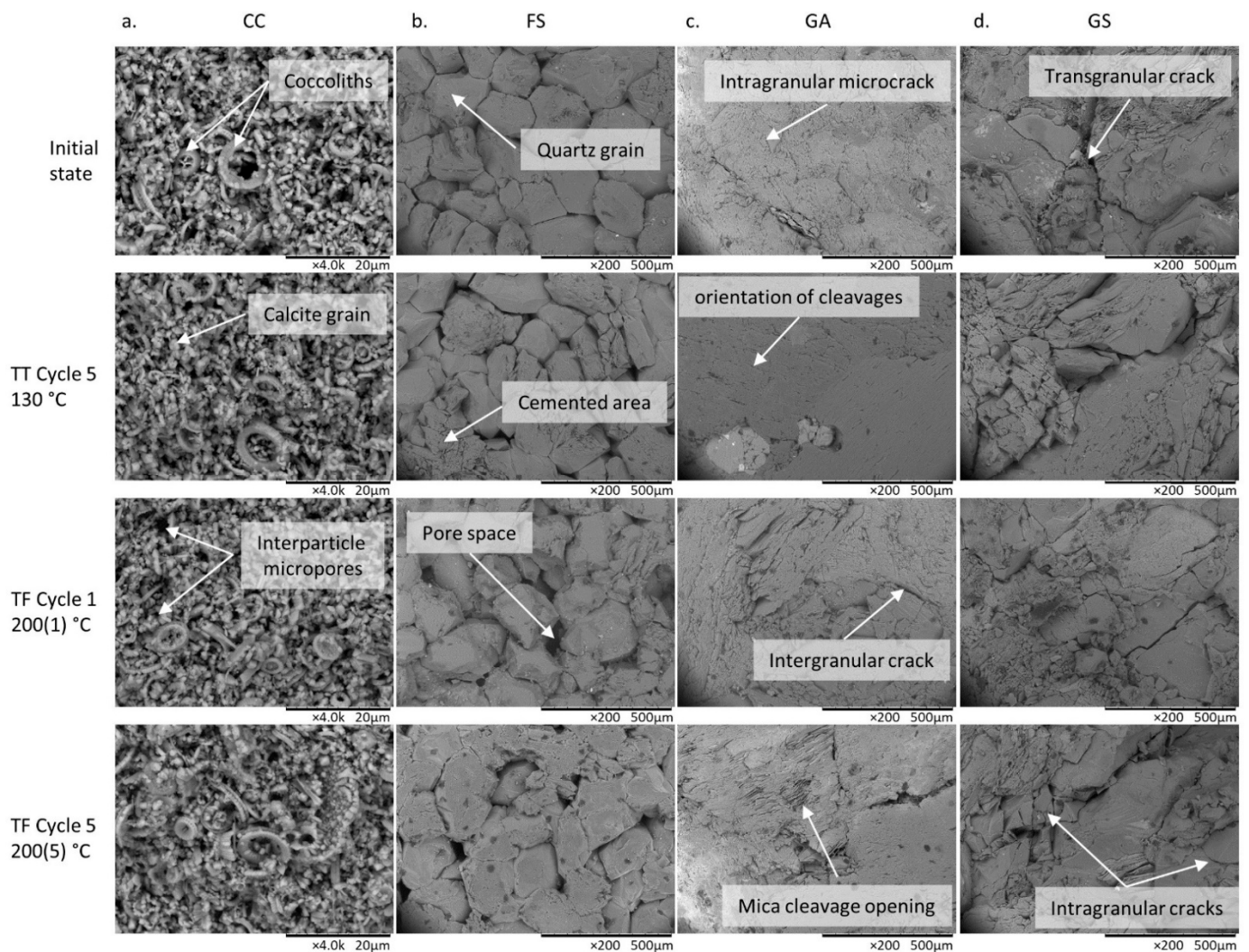


Figure 4. SEM observations of the Châlons chalk (a). CC, the Fontainebleau sandstone (b). FS, the Gris Alba granite (c). GA, and the Golden Ski granite (d). GS, in their initial state and after heating treatment. (TT: Thermal Threshold test and TF: Thermal Fatigue test).

The Fontainebleau sandstone presented different compactness, with some areas where the grains were strongly cemented. Clumps of grains were grouped and completely silicified. The crystals had a diameter between 100 and 300 μm . The shape of the porous spaces consisted of networks of channels with widths that ranged from 5 to 30 μm , although some could reach 60 μm . This pore size was sufficient to allow correct hydraulic connectivity. Capillary rectilinear ends (less than 1 μm in diameter) were found connecting the different channels of larger size. During the TT test, the rock showed some crushed crystals that invaded the intergranular porosity and the appearance of dispersed macropores, more numerous with higher temperatures (Figure 4). During the TF test, the intergranular porosity changed in two ways, with closure and widening of boundaries, revealing a pore

redistribution. Some crushed crystals were also present and intragranular microcracks became visible.

The Gris Alba granite showed predominantly intergranular cracks in the initial state. The grain size had a diameter between 4 and 6 mm [28]. The average crack width is about 8 μm [35]. After heating at 130 °C, the minerals increased in volume and the boundaries looked fused. Some pores of bigger size appeared, due to materials fracturing and material loss. The microcracks seemed angled, decreasing tortuosity and improving connectivity. At 200 °C, new microcracking appeared on the rock surface, following grain boundaries with less than 1 μm width. Mica showed a notable opening of the cleavage planes, and a material detachment was observed. The pre-existing cracks became larger and slightly wider in diameter.

The Golden Ski granite showed initially marked trans, inter, and intragranular microcracks, ranging in diameter from 5 to 50 μm . The grain size had a diameter between 2 and 4 mm [28]. After heating, minor variation was observed although new microcracks appeared especially in quartz grains. The cleavage of mica was also altered showing irregularities, even fractures that increased the roughness of the granite surface.

4.2. Mercury Injection Porosimetry (MIP)

The connected porosity of the samples before and after the thermal tests is shown in Table 2 and the variations in the pore radii access distribution in Figure 5. During heating, the differential thermal expansion coefficients of the various mineral grains cause the generation of microcracks. When rocks are held at temperature, cracks generated at this temperature remain closed. During cooling, microstructural modifications can appear [51]. If the microcrack threshold has not been reached, the minerals contracted during cooling without generating microcracks. If the thermal stress has been exceeded, microcracking occurred and increased the porosity [50].

Table 2. Porosity MIP (%) of the 4 rocks before and after treatment at different temperatures (in blue, values lower than the initial value, in red, values higher than the initial value).

	TT						TF	
	25 °C	90 °C	100 °C	110 °C	120 °C	130 °C	200(1) °C	200(5) °C
CC	37.93	42.61	37.69	39.81	40.44	40.95	40.05	40.35
FS	4.34	4.84	5.09	4.73	4.68	5.18	5.86	4.75
GA	1.05	0.87	0.95	0.96	0.95	0.80	1.59	1.39
GS	3.77	3.19	3.08	3.68	3.93	3.42	3.97	3.56

CC: Châlons chalk; FS: Fontainebleau sandstone; GA: Gris Alba granite; GS: Golden Ski granite; TT: Thermal Threshold test; TF: Thermal Fatigue test.

The Châlons chalk showed an initial porosity slightly lower than 40%, which consisted of a homogeneous microporous network with an unimodal distribution centred around 0.26 μm . During the TT, the porosity increased slightly, between 7.5 and 11%, reflected by an increase in the modal peak intensity. That indicated an augmentation of the pore volume with the same size that the initial rock. After TF, the porosity increased by about 5% with no change in the pore access radii.

The Fontainebleau sandstone had a porosity of around 4% in its initial state, with a wide unimodal distribution centred on 1 μm . The first cycle of the TT already revealed an increase in the porosity of approximately 11%, with also an evident change in the pore access radii larger than 1.5 μm . The increase was not progressive along the cycles, although the maximal value was found at 130 °C, with more than 19% increase and a pore access threshold that shifted up to almost 2 μm . In addition, a new family of bigger pores appeared from the very first heating cycle between 43 and 113 μm . For the TF cycle 1, the microstructural variations were even more remarkable, with a strong increase of 35% of pore volume and a pore threshold increase up to 3 μm . The fatigue (TF cycle 5) produced a

slight opening of the microcracks at the end of the test, with an increase of 9% in porosity compared to the initial state and an increase to 2 μm of the pore threshold.

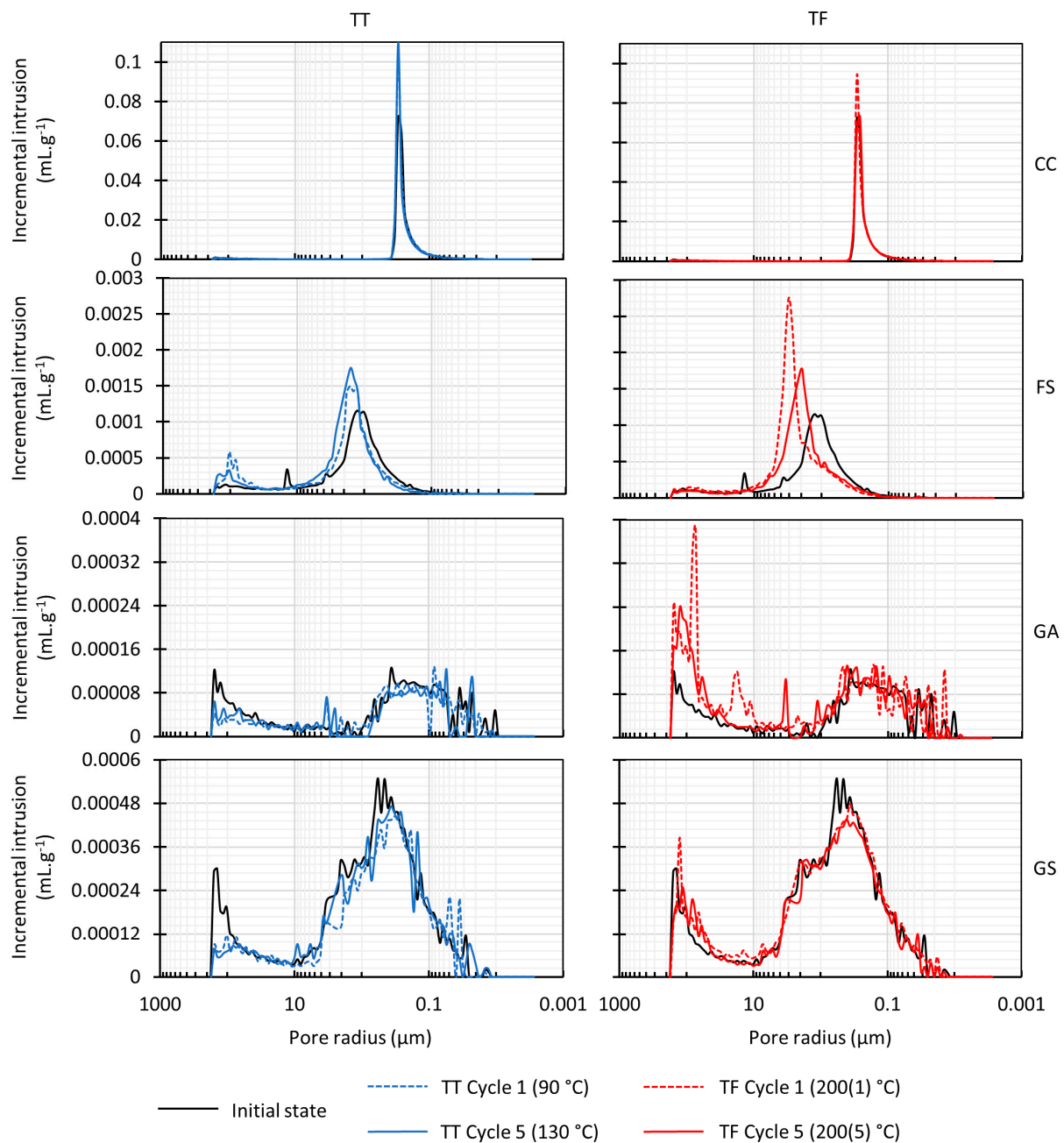


Figure 5. Pore access size distribution curves of samples before and after the first heating cycle and at the end of the TT (Thermal Threshold test) and TF (Thermal Fatigue test). CC: Châlons chalk; FS: Fontainebleau sandstone; GA: Gris Alba granite; GS: Golden Ski granite.

The Gris Alba granite presented an initial porosity volume of 1.05% and showed two main distributions, a wide micropore family with pore access radii below 1 μm and a mesopore family starting from around 10 μm . Through the TT, this rock showed a decrease in its pore volume of 17% at 90 $^{\circ}\text{C}$ and 25% at 130 $^{\circ}\text{C}$. Figure 5 exhibited a redistribution and a slight reduction in the micropore family, which could be due to the heating but also to the heterogeneity between the samples. Nevertheless, there was a clear decrease in the mesoporous family for all the heating cycles. The TF test showed a great increase in the porosity, with 51% after the first cycle and 32% at the end. The microporous family

exhibited a variation in the radii access proportion, without being possible to determine an increase or decrease graphically. A great increase in the pore access radii larger than 1 μm was measured, with the apparition of new peaks and the development of voids around 100 μm .

The Golden Ski granite had an initial porosity volume of 3.77%. This rock showed most of their pore access radii below 10 μm , with a modal value around 0.5 μm . Besides, it presented a mesopore family with a modal peak measured around 150 μm . During the TT test, this rock experimented fluctuations around the initial values, although for the temperatures of 90 °C and 130 °C a decrease of 15% and 10%, respectively, were measured. Figure 5 revealed a slight decrease in the microporous family and a disappearance of the bigger peak area, as already observed in GA. The TF test did not produce a great microstructural change in pore volume, although Figure 5 showed smoothing of the microporous family and differences between the cycles for the bigger pore area.

4.3. Capillary Absorption

The capillary water uptake results showed that 1 h was enough to calculate accurately the coefficient of capillarity. Table 3 represents the change in the coefficient C relative to the weight increase per surface unit for the two samples of each stone and each cycle.

Table 3. Capillary coefficient (C) ($\text{g}\cdot\text{m}^{-2}\cdot\text{s}^{-1/2}$) before and after heat treatments (in blue, values lower than the initial values, in red, values higher than the initial values).

	TT						TF					
	25 °C	90 °C	100 °C	110 °C	120 °C	130 °C	25 °C	200(1) °C	200(2) °C	200(3) °C	200(4) °C	200(5) °C
CC	462	451	445	451	428	411	444	466	476	486	477	489
	345	339	356	363	350	335	396	416	416	417	347	330
FS	14.8	10.1	7.6	4.3	2.8	4.3	6.7	1.6	5.1	8.6	11.1	11.4
	21.7	13.3	15.4	16.8	15.5	14.6	6.5	7.7	6.9	6.1	5.7	6.5
GA	2.2	2.1	2.2	2.7	3.5	3.7	4.8	5.0	5.0	5.4	5.3	5.6
	5.5	4.2	5.2	4.8	4.7	4.8	5.0	4.9	5.2	5.3	5.2	4.9
GS	21.9	20.0	23.3	22.5	23.4	24.7	20.2	20.8	21.1	19.0	22.5	22.8
	19.1	19.9	21.0	21.6	22.2	22.6	23.5	25.2	24.6	26.1	26.3	26.6

CC: Châlons chalk; FS: Fontainebleau sandstone; GA: Gris Alba granite; GS: Golden Ski granite; TT: Thermal Threshold test; TF: Thermal Fatigue test.

The Châlons chalk showed the highest capillary coefficient with values that varied between 350 and 460 $\text{g}\cdot\text{m}^{-2}\cdot\text{s}^{-1/2}$ in accordance with its higher porosity combined with its unimodal microporous network. During the TT test, this rock hardly showed any variation for both samples, with a maximal decrease of 11% at 130 °C. During the TF test, the chalk behaved similarly, with almost no perceptible change and only a maximal reduction of 17% on the second sample.

The Fontainebleau sandstone presented an initial capillary coefficient between 7 and 22 $\text{g}\cdot\text{m}^{-2}\cdot\text{s}^{-1/2}$. This high variability was explained by the compactness differences within the same block for this stone. For the TT, both samples showed a strong decrease in the capillary water uptake through all the heating cycles, with maximal values of 71% and 33%, respectively. For the TF test, the progression of coefficient C showed different trends for each sample. The C of the first sample decreased by 77% after its first heating but finished with an increase of 70%. The second sample hardly showed any relevant change through the test.

For the Gris Alba granite, the initial C coefficients were between 2.2 and 5.5 $\text{g}\cdot\text{m}^{-2}\cdot\text{s}^{-1/2}$ for the two samples tested. During the TT test, only the first sample showed an evident change, with a progressive increase that finished with porosity 69% higher at the end of the experiment. The other sample fluctuated slightly without being considered significant. In the TF test, this rock hardly showed any variation for both samples, with only a slight increase of 15% for one of them at the end of the test.

The Golden Ski granite exhibited initial C coefficients between 19 and 24 $\text{g}\cdot\text{m}^{-2}\cdot\text{s}^{-1/2}$, respectively. During the TT test, the variations were very little, although a progressive

increase with temperature was observed for both samples, with final increases of 12 and 18%. The TF test exhibited the same behaviour, a very slight progressive increase with cycles, and a maximal value of 13% at the end of the test.

4.4. Wet Fringe

The wet fringe was observed and measured by the naked eye during the capillary test. IRT allowed us to observe and quantify not only the wet fringe but also the water distribution within the outer layers of the studied stones. The main fact extracted from the IRT images was that porous and fissural rocks behaved differently. In both cases, three zones were defined (Figures 6 and 7):

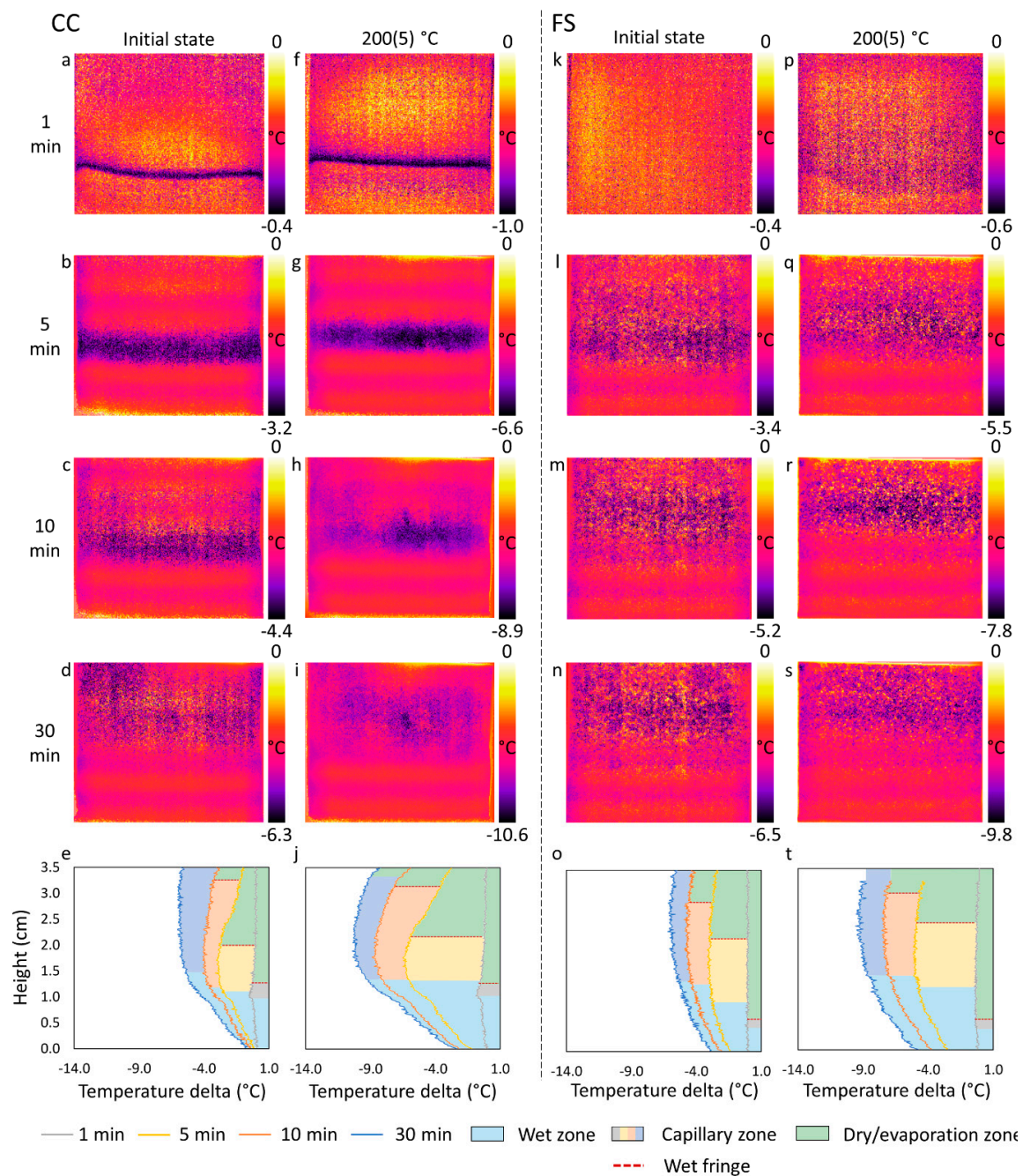


Figure 6. Subtracted IRT images of CC (Châlons chalk) and FS (Fontainebleau sandstone) at their initial state (a–d,k–n) and after 5 cycles of TF (Thermal Fatigue test) (200(5) °C) (f–i,p–s) obtained by subtracting thermograms at 1, 5, 10, and 30 min from the initial state. Vertical temperature profiles are plotted from the IRT images (e,j,o,t).

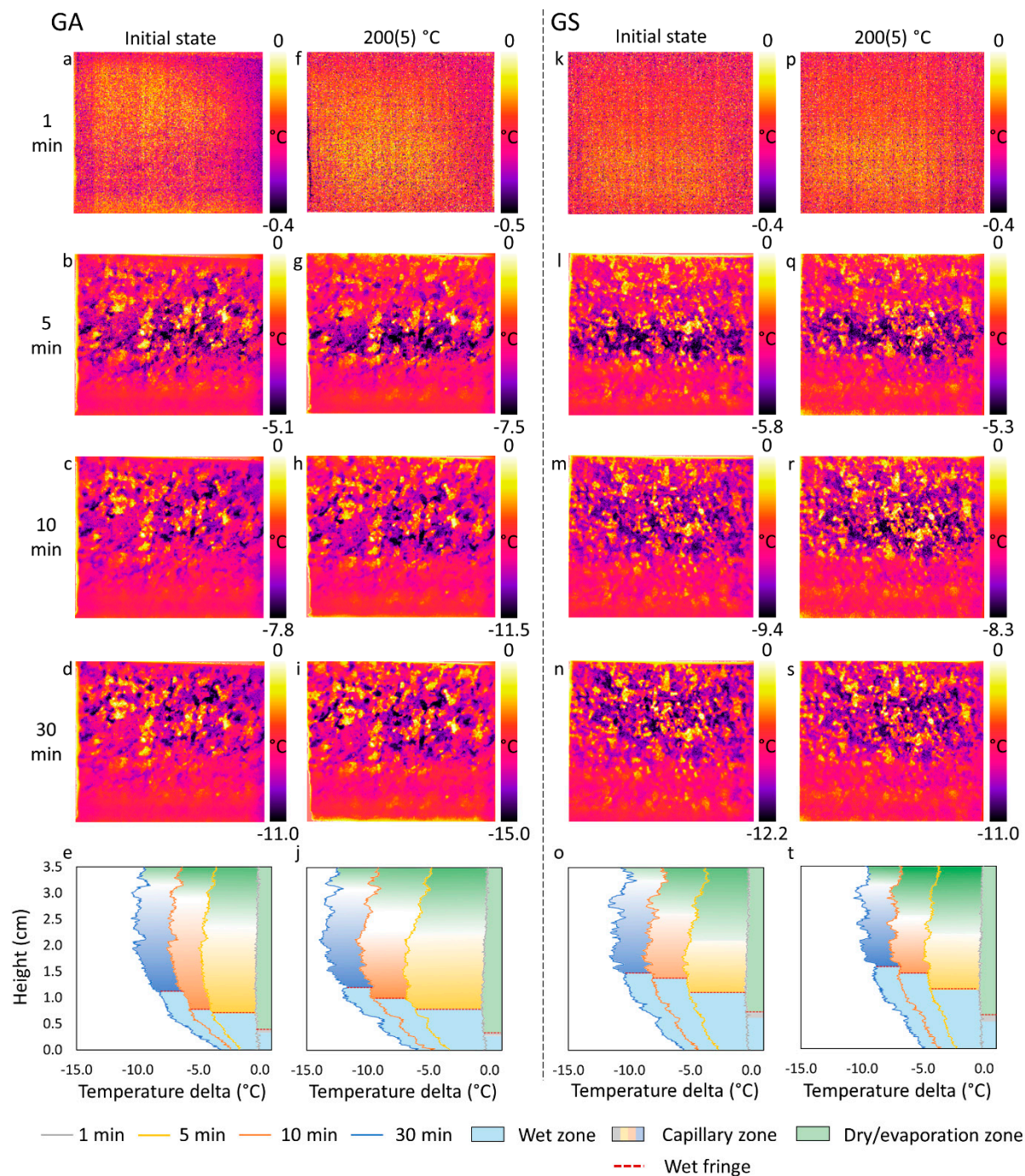


Figure 7. Subtracted IRT images of GA (Gris Alba granite) and GS (Golden Ski granite) at their initial state (a–d,k–n) and after 5 cycles of TF (Thermal Fatigue test) (200(5) °C) (f–i,p–s) obtained by subtracting thermograms at 1, 5, 10, and 30 min from the initial state. Vertical temperature profiles are plotted from the IRT images (e,j,o,t).

- (i) The wet zone, where the water filled the void system almost instantly and the temperature between the fluid and the rock equilibrated rapidly. The rock surface was wet.
- (ii) The capillary zone, an area of inner water migration evidenced by a homogeneous mineral cooling.
 1. In the sedimentary stones, this zone was also observed by the naked eye as wet. The upper part of the capillary zone corresponded to the visible wet fringe.
 2. In the granites, this zone was dry although a strong mineral cooling produced only by water effect was observed by IRT. The bottom part of the capillary zone corresponded to the visible wet fringe.

(iii) The dry/evaporation zone, the upper part that was not invaded by water and cooled freely by air contact. In some cases, an evaporation zone when the water already reached the top of the sample.

Vertical profiles were graphed to delimit these zones at different times of the capillary water uptake test (Figures 6 and 7).

Figure 6 showed the three parts of the sedimentary stones behaviour during capillary water uptake. A homogeneous wet zone that cooled quickly, a capillary zone marked by the distribution of the dark colour, and an upper dry zone in which the cooling took place at a moderate rate.

For the Châlons chalk, the IRT images revealed that for the fresh rock, after 1 min of water contact, the wet fringe was a thin dark line at around 1 cm height (Figure 6a). After 5 min, the wet zone was slightly spread at the mid-height of the sample, although the upper part of the dark line corresponded to the wet fringe observed visually around 2.2 cm. After 10 min, the water was well distributed in the whole sample in the IRT images (Figure 6a–e) and also observed by the naked eye. At the end of TT, the IRT images were similar to those from the same time-lapse at the initial state, with a slight difference due to the increase in the capillary zone height after 5 min. The thermal profile graphed a faster cooling in the tested sample and an evaporation phase at the upper part. During the last cycle of the TF test (Figure 6f–j), after 5 min, the wet fringe was measured slightly higher than the initial state and after 30 min, the sample saturation and an evaporation area were clearly observed.

The water behaviour in Fontainebleau sandstone is shown in Figure 6k–t. After 1 min, no changes were perceived on the IRT image. Nevertheless, at 5 min the wet fringe was clearly observed with the naked eye at around 2 cm, that in the IRT image included the wet zone (of about 0.5 cm) and the capillary moist zone (1.5 cm), in which the water circulated and advanced to the top with the time (Figure 6o). In the TT test, the wet fringe appeared from minute 1, and its migration together with the rock cooling area to the upper part of the sample was observed. In the TF test (Figure 6p–t), the wet zone rose higher and the cooling of the capillary area to the top of the sample at the end of the test was evident. The profiles were more homogeneous and smoother than the chalk ones, so the combination of the naked eye, the profiles, and the IRT images were needed to establish the interpretation of the water migration.

Figure 7 showed the three parts of granite behaviours. The wet zone presented homogeneous colours in the IRT image without mineral differentiation and an abrupt cooling in the temperature profile. The capillary zone was defined as a smooth progression from the homogeneous wet zone to a zone with differential mineral cooling. The dry zone was clearly delimited during the first minutes in the IRT images. Afterward, air and water cooling were mixed and only the profiles helped to establish the limits.

The fresh Gris Alba granite exhibited in IRT a slight and homogeneous cooling after 1 min. The vertical temperature profiles and the IRT images showed that the wet zone increased clearly from about 0.5 mm height at 5 min to around 1 mm at 30 min (Figure 7a–j), in agreement with the wet fringe observed by the naked eye. The upper part of the capillary zone can be defined as the darkest band at the middle of the IRT image at 5 min, and despite the lack of visible moisture on the rock surface, the water possibly reached the top of the sample after 30 min, with regard to the cooling phenomena. During both TT and TF tests, the IRT images were similar to the fresh stone, although, after 5 min, the central area cooled by the water rise was better defined. The profiles showed a marked increase in the cooling rate and a bottom zone with more pronounced mineral differences.

The Golden Ski granite exhibited a comparable behaviour to GA, with a homogeneous cooling during the first minute (Figure 7k). The wet zone was established approximately at the same height at 5 min and slightly higher at 10 and 30 min, also in agreement with visual observations. The capillary zone migrated to the top of the sample. At the end of TT and the TF test (Figure 7p–t), the trend was the same, with a similar differential mineral cooling.

4.5. Cooling Rate Index (CRI)

The CRI corresponded to the slope of the temperature average variation during the first 10 min of cooling according to [42]. As the CRI assesses the cooling of the dry zones, the average temperature was recorded in the upper part of the samples (Figure 3). Only for the chalk where the capillary rise was very fast, the CRI was calculated during the first 5 min. Higher values of CRI meant fast cooling (Table 4).

Table 4. Cooling rate indexes ($^{\circ}\text{C}\cdot\text{min}^{-1}$) of the 4 rocks before and after treatment at different temperatures (in blue, values lower than the initial values, in red, values higher than the initial values).

	TT						TF		
	25 $^{\circ}\text{C}$	90 $^{\circ}\text{C}$	100 $^{\circ}\text{C}$	110 $^{\circ}\text{C}$	120 $^{\circ}\text{C}$	130 $^{\circ}\text{C}$	25 $^{\circ}\text{C}$	200(1) $^{\circ}\text{C}$	200(5) $^{\circ}\text{C}$
CC (CRI5)	0.26	0.26	0.42	0.29	0.53	0.51	-	0.11	0.72
FS (CRI10)	0.43	0.62	0.57	0.59	0.75	0.86	-	0.48	0.71
GA (CRI10)	0.31	0.05	0.49	0.63	0.71	0.6	0.67	0.78	0.89
GS (CRI10)	0.90	0.56	0.71	0.7	0.71	0.64	0.77	0.83	0.68

CC: Châlons chalk; FS: Fontainebleau sandstone; GA: Gris Alba granite; GS: Golden Ski granite; TT: Thermal Threshold test; TF: Thermal Fatigue test.

The Châlons Chalk showed the lowest cooling kinetics compared to all the stones. Despite its high porosity, the small pore sizes led to a very low thermal diffusivity of only $0.59\text{ mm}^2\cdot\text{s}^{-1}$ [58]. During the TT, the cooling rate increased up to double, which indicated a change of the surface properties. The variations through the TF also revealed an increase in the cooling velocity.

The Fontainebleau sandstone showed an initial CRI of intermediate value between the stones. The main parameters involved in its kinetics are the low porosity and the high quartz content that increase diffusivity in relation to a standard sandstone (diffusivity between 1.13 and $1.67\text{ mm}^2\cdot\text{s}^{-1}$) [58]. During the TT, there was an increase in the cooling kinetics up to double of the initial values indicating a variation in outer layers porosity. The temperature was too low to produce a mineralogical change. On the other hand, the TF revealed an increase in the cooling velocities that confirmed the microstructural change.

The Gris Alba showed a low initial CRI, according to its low porosity and quartz content. A standard granite has a diffusivity of around $1.13\text{ mm}^2\cdot\text{s}^{-1}$ while a low porosity granite can have a lower one up to $0.77\text{ mm}^2\cdot\text{s}^{-1}$. At the end of the TT test, the CRI values doubled, reaching the highest ones at $120\text{ }^{\circ}\text{C}$. The fatigue at $200\text{ }^{\circ}\text{C}$ produced a slight increase in the cooling rate, although enough to ensure that a microcracking was taking place, at least on the surface.

The Golden Ski granite showed the highest CRI among the studied stones. That was probably due to its initial alteration with wide and long microcracks. A high permeability granite can reach diffusivity values of around $1.77\text{ mm}^2\cdot\text{s}^{-1}$. During the TT, the CRI decreased for all the heating cycles, with a percentage of around -30% at the end of the test. The fatigue also led to a decrease in the cooling kinetics that implied an opposite behaviour than the rest of the rocks.

5. Discussion

There are several parameters such as porosity, mineralogical composition, anisotropy, and granulometry that influence the thermal sensitivity of the rocks [59]. In addition, other properties related to the porous network, such as pore volume, pore access radii, tortuosity or connectivity, condition the water flow. During heating, the creation of microcracks and the thermal expansion of minerals are two contradictory phenomena in the evolution of the microstructure, and the variation of all the above-mentioned parameters leads to differences in their thermal and hydric properties. The degree of cracking depends mainly on temperature and mechanical strains, mineralogical composition, and particle size distribution [60]. In addition, it is possible that microcracks appear during the first cycles, even with a low heating rate (1 to $2\text{ }^{\circ}\text{C}\cdot\text{min}^{-1}$) [61].

5.1. Thermal Threshold Test (TT)

The progressive heating of the selected stones up to 130 °C produced changes more or less remarkable depending on the initial microstructure and composition quantified by MIP, capillary water uptake, and CRI (Figure 8).

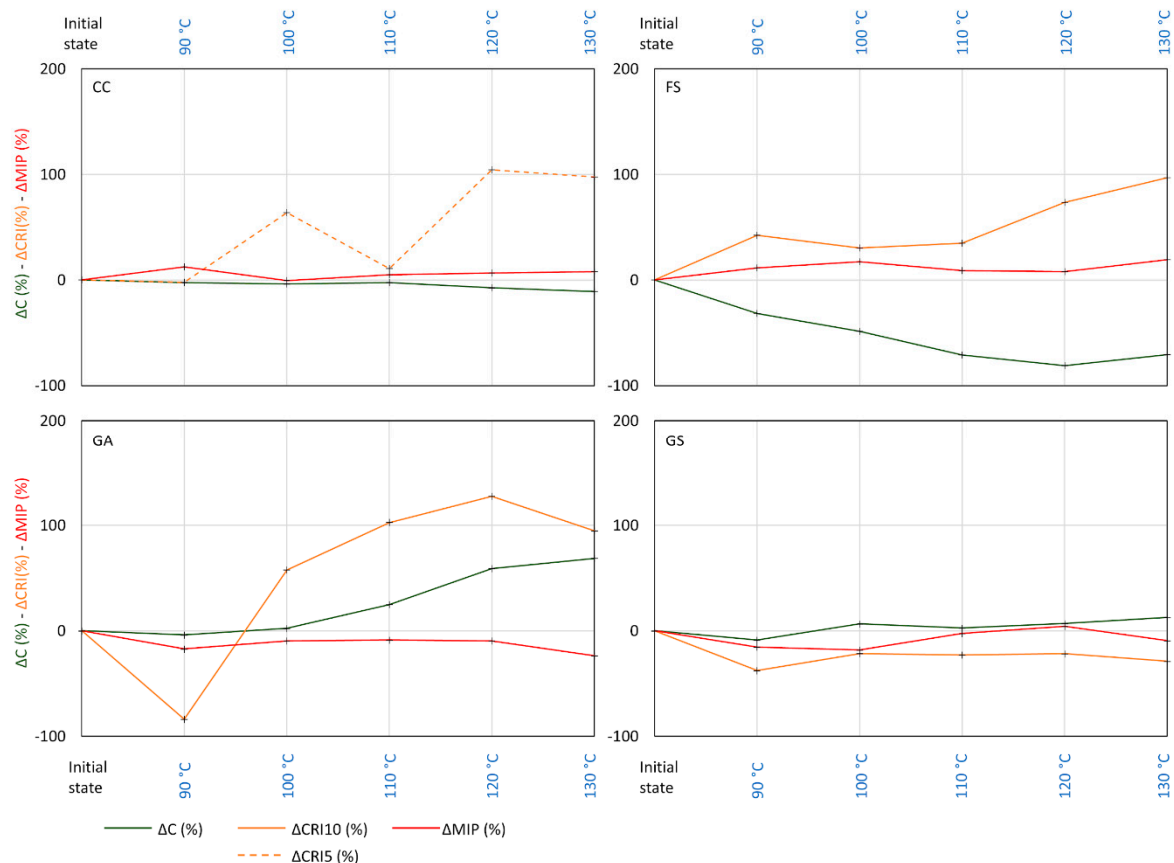


Figure 8. Variations of the capillary coefficient (C), the cooling rate index (CRI), and the porosity (MIP) along the Thermal Threshold test (TT).

The Châlons chalk (CC) is a microporous rock with a void volume of around 40%. That implies an easy readjustment of the calcite expansion during heating that avoids the microcrack formation. Thus, very slight changes were observed in the properties related to their microstructure, that is, capillary water absorption and MIP (Figure 8).

Despite the calcite solubility, the interaction times between this mineral and water were too short during the tests to produce any chemical alteration on chalks [62,63] or uniform dissolution between intergranular contacts [64]. Most of the studies on the behaviour of chalk with increasing temperatures (around 100–130 °C) revealed that no mechanical variations were produced [3,65–69], although a few times a slight variation of the elastic modulus was quantified [64,66,70]. However, the tensile forces on the outer layers during heating may produce weakness in some boundaries that may lead to a granular disaggregation or crushing on the surface [46]. The SEM observations after treatment showed that the porous structure of the chalk consisted of a more heterogeneous zone with the grouping of numerous particles in the same place. The surface roughness for natural chalk is on the order of only a few micrometers and cycles of wetting and drying can erode its surface [71]. This erosion was mainly due to the detachment of the particles. These observations suggest that the study of the surface roughness of the chalk is an important parameter for evaluating the cooling rate index (CRI) because it depends on the exchanges between the surface and the environment. An augmentation in roughness is a valuable

hypothesis to explain the increase in the CRI after some heating cycles and capillary tests (Figure 9a).

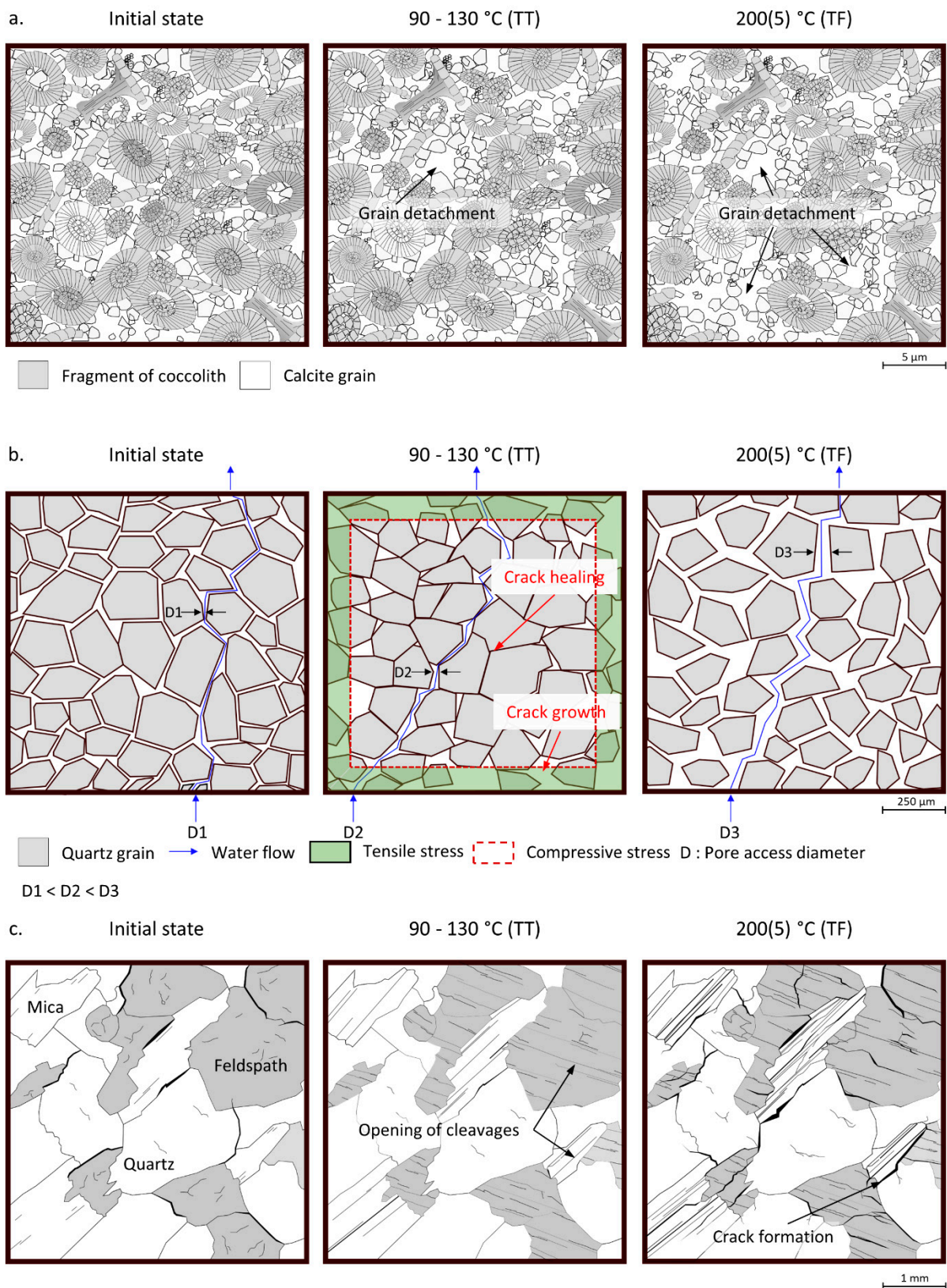


Figure 9. Diagram of the evolution of the porous 2D network of the Châlons chalk (a), Fontainebleau sandstone (b), and Gris Alba (c) according to the temperature.

The Fontainebleau sandstone (FS) is composed mainly of quartz, a mineral with high and anisotropic thermal expansion. Microstructural variations through TT were observed with a slight increase in the pore volume and pore access radii under 140 μm and a decrease in the capillary water uptake kinetics. Acoustic emission studies revealed microcracking in sandstones at temperatures as low as 65 $^{\circ}\text{C}$ [72] and 100 $^{\circ}\text{C}$ [73], while [74] discovered grain boundary cracking at temperatures under 125 $^{\circ}\text{C}$. The trend of this microstructural variation is aleatory, with an increase in crack density measured by [75] and a decrease in porosity by [76]. Localisation, connectivity to porosity, and the opening of microcracks are important parameters in the analysis of fluid transfer [77]. It has been observed that the water rises more slowly in the wider parts of the porous network of the Fontainebleau sandstone [47]. The SEM images (Figure 4) and the increase in the CRI (Figure 8) helped to schematize the FS behaviour during the TT test (Figure 9b). In its initial state, the flow of capillary water uptake was regular thanks to the homogeneous and continuous distribution of the entire pore volume. The size of the flow paths was small (radius centred about 1 μm) although pores of smaller size were present because of the strongly cemented areas locally. As described by [46], a fine zone of microcracking on the outside of the samples (tensile stresses) and a thick zone of crack closure in the center (compressive stresses) can be observed on rocks following thermal stress. Between 90 and 130 $^{\circ}\text{C}$, intergranular porosity healing may occur at the center of the sample in the compression zone, accentuated by the high thermal expansion of quartz [78]. This change led to a decrease in water absorption. The outer tensile zone readjusted the quartz grains and widened the space between the grains. The presence of macropores increased the temperature exchanges with the external environment, which enhanced the cooling rate (CRI).

The Gris Alba (GA) is a fresh granite with low quartz content and low porosity. During heating, GA exhibited an increase in C and CRI, while the MIP showed a reduction in pores around 100 μm . The SEM images (Figure 4c) revealed a more compacted microstructure, with the disappearance or the fusion of microcracks, which explained the MIP values, but also a crack redistribution with the connection of oriented microcracks, the cleavage opening of mica sheets, and the reduction in tortuosity (Figure 9c), with the consequent augmentation of C. This higher connectivity and the mica opening influenced also positively the CRI. The opening of pre-existing cracks has already been characterised in granite at temperatures below 130 $^{\circ}\text{C}$ [23,24,26,79]. The MIP values nevertheless show a slight decrease in the pore volume after the first cycle. This pore closure at 90 $^{\circ}\text{C}$ was observed in particular with a reduction in the access larger than 10 microns. Thermal tests have been shown to induce more modification of the macroporosity than the microporosity for granites similar to GA (low porosity) [60].

The Golden Ski granite (GS) is a weathered granite with high cracking and clays. In addition, its high mica proportion helps to adapt to the stress produced during temperature rise. Due to this fact, few changes were observed in GS during TT, except for a slight decrease in the CRI, explained by the increase in the volume of certain minerals, such as quartz, that may close the bigger microcracks.

5.2. Thermal Fatigue Test (TF)

The repetition of heating cycles (TF) showed fewer fluctuations than the TT, although some rocks were very sensitive to this thermal regime (Figure 10).

The behaviour of the chalk to the TF test was similar to the TT test, with no variations in its microstructure but a grain crushing and loss of material on the surface, which produced only an increase in the CRI (Figures 9a and 10). During a temperature increase on chalk, the calcite observed at SEM is likely to expand freely [80], however, none of these dilatations or mineralogical modifications have generated significant changes in the bulk microstructure of the chalk [3].

The Fontainebleau sandstone (FS) showed a microstructural redistribution during the first heating at 200 $^{\circ}\text{C}$, with an increase in porosity measured by MIP, and a decrease in C. Through the thermal fatigue, FS experienced better connectivity of the porosity thanks

to the creation of intergranular cracks (Figure 4) which lead to a higher C. Actually, the porous volume is connected in 3D with a larger intergranular matrix size than in the initial state (Figure 9b). The big macropores and some grain detachment contributed to the augmentation of cooling velocities through the thermal cycles (Figure 10).

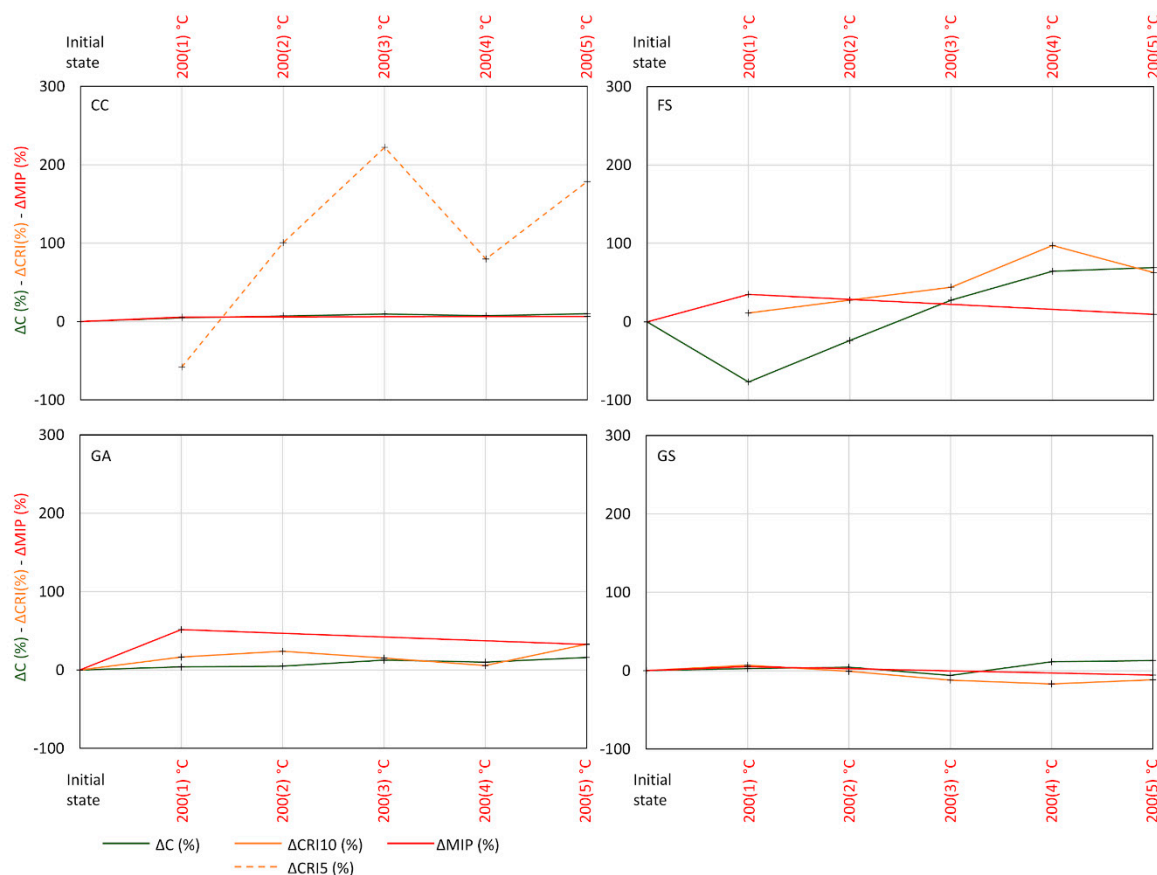


Figure 10. Relationship between the capillary coefficient (C), the cooling rate index (CRI), and the MIP porosity for the Thermal Fatigue test (TF).

From the very first heating at 200 °C, the Gris Alba granite (GA) showed a significant modification of its porous network, observed by SEM and quantified by MIP, with a more intense microcracking in feldspar [60] and an increase in the pore radius access greater than 100 μm. The pores with access radii greater than 10 μm constituted preferential flow paths during capillary water uptake. Nevertheless, they were not the largest part of the porous network of GA, which explained the little variation in C (Figure 10). During the following heating cycles, all the properties as well as the observations did not show great changes, indicating that the first heating produced a great redistribution in the GA microstructure and that it was not affected by thermal fatigue.

Similar to the TT test, the microstructural parameters of the Golden Ski granite (GS) hardly changed through the TF test, although for lower temperatures and fatigue of 30 cycles, an increase in porosity was reported [28]. Only the CRI experienced a decrease explained by a mineral expansion that closed the bigger cracks and clay remobilisation that occluded some of the surface voids [21]. The clays placed on the edge of the pore walls allowed the continuous water circulation (Robert, 2004) that was in agreement with the CRI and capillary results (Figure 10).

5.3. IRT as a Tool to Detect Microstructural Changes

The capillary water uptake can be followed by IRT since the variation of emittance in wet porous materials allows the movement of water to be visualised on stone sur-

faces [36,81]. Regarding the fresh stones, the thermographs showed a correlation between porosity and water absorption by capillarity [37,38], with a faster rise in the chalk, whilst slower in the sandstone and the granites, with a stabilisation of the wet fringe at the middle of the samples.

The capillary water uptake test, and more precisely the penetration index, determined a bottom wet part, in which the water circulates, and an upper dry zone, separated by its observable moist surface (wet fringe). The IRT monitoring made it possible to define these two visible zones, with different migration interpretations for porous and fissural rocks. During the first minutes, the water–rock interaction reached a very fast temperature equilibrium at the bottom part of the sample. From that, the void network controlled the wet fringe movement (Figure 11).

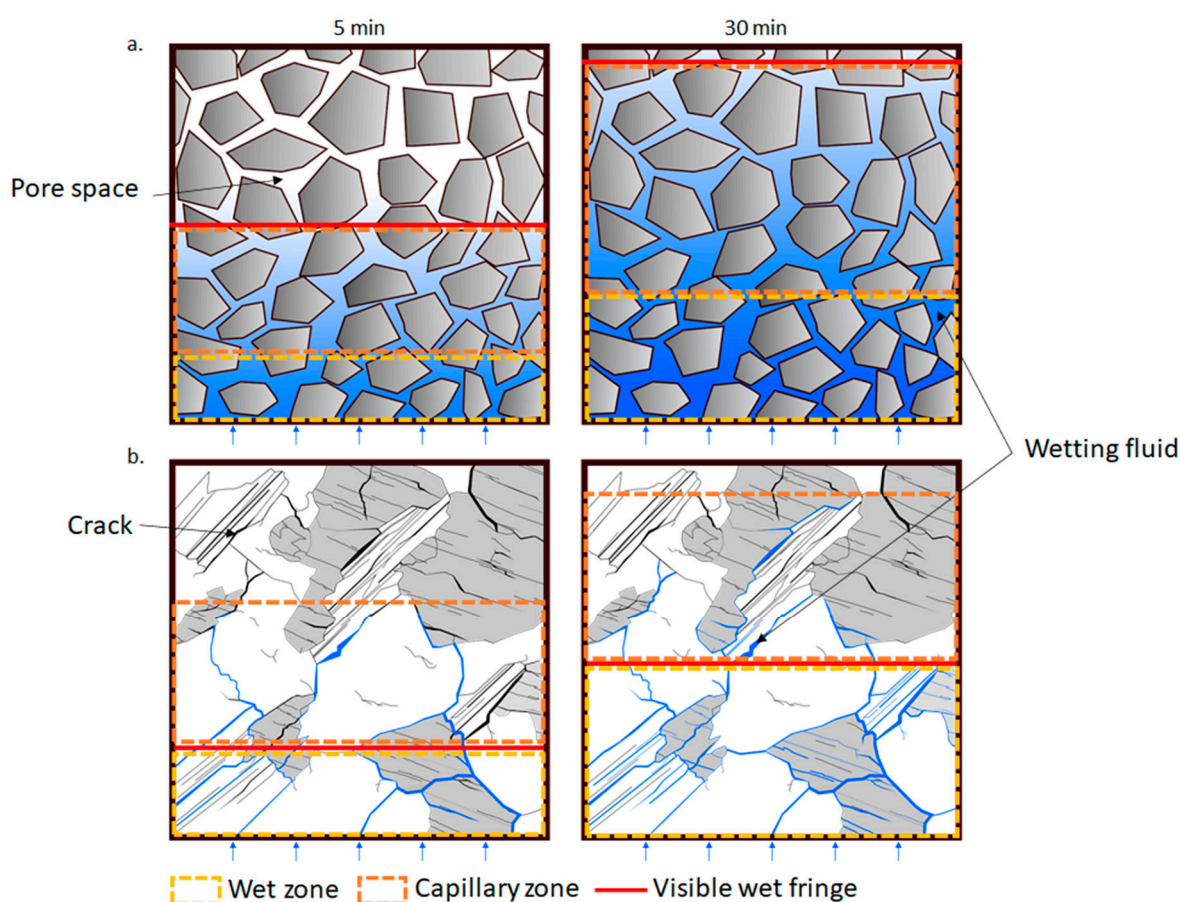


Figure 11. Fluid circulation in porous media. (a) Granular rock. (b) Polycrystalline rock.

For sedimentary rocks (Figure 6e,j,o,t), the water contained in the pore system rose and occupied the pore space uniformly so that the wet fringe migrated according to the water filling, delimited by the upper part of the capillary zone (Figure 11a). A better arrangement and connection of the grains favour the kinetics of internal migration of the fringe and the cooling by water. When the wet fringe reached the top, the sample compensated for the loss of water through evaporation.

Fissural rocks presented a heterogeneous pattern. The profiles in Figure 7e,j,o,t and the visual observation revealed similar evolution for the wet zone and wet fringe. The interconnected cracks of the porous network became saturated from the first minutes. That included the wet zone and the capillary zone. The water saturation continued with the occupation of the transverse cracks, showing a heterogeneous migration of the wet fringe through the first 1.5 cm (Figure 11b). Monitoring the rise in water by capillarity using the IRT

detects variations in the microstructure (cooling/variation of the wet fringe) but without quantification.

Infrared thermography also allowed us to quantify the cooling rate index for the upper part of the sample, by simple exchange with the environment. This parameter is well correlated to porosity for stones with a void volume over 10%, although with approximate values that allow us only to divide into groups (10%, 15%, 20%) [41,42,82]. The studied rocks did not follow these statements. For fissural rocks and special microporosity rocks, such as chalk, the surface roughness and the microcrack connectivity will play a more important role than the porosity itself. The CRI of granite with 1% porosity and sandstone with 5% were similar, while the CRI of high microporous chalk was very low and the CRI of a weathered granite with the same porosity as the sandstone was three times.

The CRI varied during the heating cycles, although not in the same sense that the bulk microporosity. However, the changes on the network observed by SEM explained completely the cooling rate behaviour. That indicated that the CRI was not a probe of the small development of microcracking within the rock but a good indicator of the damage to the outer layers, from which the temperature changes started.

6. Conclusions

The comparison of four rocks with differences in mineralogy and porous networks submitted to increasing temperature and Thermal Fatigue tests was achieved using several methods, including an innovative approach as infrared thermography.

The influence of temperature on the chalk microstructure was weak. Nevertheless, the instability of the particles and the loss of material increased the surface roughness and consequently the thermal exchange with the environment, translated by a rise in its cooling rates.

The progressive heating produced a compressive strain on the sandstones' core measured and observed as an internal closure of its porosity and tensile stress on the surface that increased the cooling rates. With fast and repetitive heating, this rock created an irreversible crack development measured and observed with all the techniques.

At the end of the Thermal Threshold tests, the fresh granite showed new intra- and intergranular-oriented microcracks and cleavage opening, favouring the interconnection of the network and the fluid flow. Heating up to 200 °C only produced a slight microstructural change compensated by a mineral residual strain. The weathered granite showed fewer variations through the tests due to the clay and mica adaptation to the deformations.

Infrared thermography evidenced the variations produced by thermal stresses. The cooling rate index (CRI) did not correlate the stones to their bulk porosity although it gave information in agreement with the SEM observations about the surface changes.

The evolution of thermograms during water uptake made it possible to interpret two capillary diffusion mechanisms depending on the rock type. The homogeneous and interconnected structure of the granular rocks showed a homogeneous rise of the wet fringe and stone cooling as the pores were filled, that is the visible wet fringe corresponded to the water rise. The heterogeneous fissural media exhibited a complex water filling, in which the visible wet fringe was conditioned by a wet zone close to saturation and not by the height of the water rise. The water uptake was carried out firstly in the connected microcracks, then in a second step, the filling of water continued in the transverse cracks less connected to the entire network. This filling marked the wet fringe evolution.

These preliminary results allow IRT to be considered as a promising technique for rock characterization, although more research is needed on CRI parameter and capillary water uptake for a more accurate interpretation of crack and pore networks.

Author Contributions: Conceptualization, T.J. and P.V.; Investigation, T.J., I.H. and M.J.-B.; Writing—original draft, T.J. and P.V.; Resources, Y.G.; Supervision, P.V.; Writing—review & editing, T.J., P.V. and C.T.-S. All authors have read and agreed to the published version of the manuscript.

Funding: This research received no external funding.

Institutional Review Board Statement: Not applicable.

Informed Consent Statement: Not applicable.

Data Availability Statement: Data is contained within the article.

Acknowledgments: We would like to express our deep gratitude to our partners from the University of Reims Champagne-Ardenne (France) and La Région Grand Est for their kind scientific collaboration and participation in the development of this project.

Conflicts of Interest: The authors declare no conflict of interest.

References

- Bai, B.; He, Y.; Li, X. Numerical study on the heat transfer characteristics between supercritical carbon dioxide and granite fracture wall. *Geothermics* **2018**, *75*, 40–47. [\[CrossRef\]](#)
- Brehme, M.; Blöcher, G.; Cacace, M.; Kamah, Y.; Sauter, M.; Zimmermann, G. Permeability distribution in the Lahendong geothermal field: A blind fault captured by thermal–hydraulic simulation. *Environ. Earth Sci.* **2016**, *75*, 1088. [\[CrossRef\]](#)
- Nadah, J.; Skoczylas, F.; Bakowski, S. Effet de la température sur le comportement mécanique d’une craie du Nord de la France. In *Congrès Français de Mécanique*; AFM, Maison de la Mécanique: Courbevoie, France, 2009.
- Witherspoon, P.A.; Nelson, P.; Doe, T.; Thorpe, R.; Paulsson, B.; Gale, J.; Forster, C. Rock Mass Characterization for Storage of Nuclear Waste in Granite. *IEEE Trans. Nucl. Sci.* **1980**, *27*, 1280–1290. [\[CrossRef\]](#)
- Andreassen, K.A. *Temperature Influence on Rock Mechanical Properties: High-Porosity, Low-Cemented Chalk*; Technical University of Denmark (DTU): Lyngby-Taarbæk, Denmark, 2011.
- Heuze, F.E. High-temperature mechanical, physical and Thermal properties of granitic rocks—A review. *Int. J. Rock Mech. Min. Sci. Geomech. Abstr.* **1983**, *20*, 3–10. [\[CrossRef\]](#)
- Lion, M.; Skoczylas, F.; Ledesert, B. Effects of heating on the hydraulic and poroelastic properties of bourgogne limestone. *Int. J. Rock Mech. Min. Sci.* **2005**, *42*, 508–520. [\[CrossRef\]](#)
- Somerton, W.H.; Mehta, M.M.; Dean, G.W. Thermal Alteration of Sandstones. *J. Pet. Technol.* **1965**, *17*, 589–593. [\[CrossRef\]](#)
- Takarli, M.; Prince-Agbodjan, W. Temperature Effects on Physical Properties and Mechanical Behavior of Granite: Experimental Investigation of Material Damage. *JAI* **2008**, *5*, 1–13. [\[CrossRef\]](#)
- Sajid, M.; Coggan, J.; Arif, M.; Andersen, J.; Rollinson, G. Petrographic features as an effective indicator for the variation in strength of granites. *Eng. Geol.* **2016**, *202*, 44–54. [\[CrossRef\]](#)
- Faÿ-Gomord, O.; Soete, J.; Katika, K.; Galaup, S.; Caline, B.; Descamps, F.; Lasseur, E.; Fabricius, I.L.; Saiag, J.; Swennen, R.; et al. New insight into the microtexture of chalks from NMR analysis. *Mar. Pet. Geol.* **2016**, *75*, 252–271. [\[CrossRef\]](#)
- Madland, M.V.; Hiorth, A.; Omdal, E.; Megawati, M.; Hildebrand-Habel, T.; Korsnes, R.I.; Evje, S.; Cathles, L.M. Chemical Alterations Induced by Rock-Fluid Interactions When Injecting Brines in High Porosity Chalks. *Transp. Porous Media* **2011**, *87*, 679–702. [\[CrossRef\]](#)
- Rosenbrand, E.; Haugwitz, C.; Jacobsen, P.S.M.; Kjoller, C.; Fabricius, I.L. The effect of hot water injection on sandstone permeability. *Geothermics* **2014**, *50*, 155–166. [\[CrossRef\]](#)
- Somerton, W.H.; Janah, A.H.; Ashqar, P.I. Thermal Expansion of Fluid Saturated Rocks Under Stress. In Proceedings of the SPWLA 22nd Annual Logging Symposium, Mexico City, Mexico, 23–26 June 1981.
- Wang, Y.; Dusseault, M.B. A coupled conductive-convective thermo-poroelastic solution and implications for wellbore stability. *J. Pet. Sci. Eng.* **2003**, *38*, 187–198. [\[CrossRef\]](#)
- Ding, Q.-L.; Ju, F.; Mao, X.-B.; Ma, D.; Yu, B.-Y.; Song, S.-B. Experimental Investigation of the Mechanical Behavior in Unloading Conditions of Sandstone After High-Temperature Treatment. *Rock Mech. Rock Eng.* **2016**, *49*, 2641–2653. [\[CrossRef\]](#)
- Yang, S.-Q.; Ranjith, P.G.; Jing, H.-W.; Tian, W.-L.; Ju, Y. An experimental investigation on thermal damage and failure mechanical behavior of granite after exposure to different high temperature treatments. *Geothermics* **2017**, *65*, 180–197. [\[CrossRef\]](#)
- Berest, P.; Vouille, G. Notions de base de la thermomécanique. In *La Thermomécanique des Roches, BRGM Manuels Méthodes 16*; Berest, P., Weber, P., Eds.; Bureau de Recherches Géologique et Minières: Orléans, France, 1988; pp. 68–101.
- Chayé d’Albissin, M.; Sirieys, P. Thermal deformability of rocks: Relation to rock structure. In *Rock at Great Depth*; Maury & Fourmaintraux: Balkema, Rotterdam, 1989; pp. 363–370.
- Gómez-Heras, M.; Smith, B.J.; Fort, R. Surface temperature differences between minerals in crystalline rocks: Implications for granular disaggregation of granites through thermal fatigue. *Geomorphology* **2006**, *78*, 236–249. [\[CrossRef\]](#)
- Vázquez, P.; Siegesmund, S.; Alonso, F.J. Bowing of dimensional granitic stones. *Environ. Earth Sci.* **2011**, *63*, 1603–1612. [\[CrossRef\]](#)
- Darot, M.; Gueguen, Y.; Baratin, M.-L. Permeability of thermally cracked granite. *Geophys. Res. Lett.* **1992**, *19*, 869–872. [\[CrossRef\]](#)
- Géraud, Y.; Mazerolle, F.; Raynaud, S. Comparison between connected and overall porosity of thermally stressed granites. *J. Struct. Geol.* **1992**, *14*, 981–990. [\[CrossRef\]](#)
- Lin, W. Permanent strain of thermal expansion and thermally induced microcracking in Inada granite. *J. Geophys. Res. Solid Earth* **2002**, *107*, ECV 3-1–ECV 3-16. [\[CrossRef\]](#)
- Meredith, P.G.; Atkinson, B.K. Fracture toughness and subcritical crack growth during high-temperature tensile deformation of Westerly granite and Black gabbro. *Phys. Earth Planet. Inter.* **1985**, *39*, 33–51. [\[CrossRef\]](#)

26. Yu, Q.L.; Ranjith, P.G.; Liu, H.Y.; Yang, T.H.; Tang, S.B.; Tang, C.A.; Yang, S.Q. A Mesostructure-based Damage Model for Thermal Cracking Analysis and Application in Granite at Elevated Temperatures. *Rock Mech. Rock Eng.* **2015**, *48*, 2263–2282. [\[CrossRef\]](#)
27. Janio de Castro Lima, J.; Paraguassú, A.B. Linear thermal expansion of granitic rocks: Influence of apparent porosity, grain size and quartz content. *Bull. Eng. Geol. Environ.* **2004**, *63*, 215–220. [\[CrossRef\]](#)
28. Vázquez, P.; Sánchez-Delgado, N.; Carrizo, L.; Thomachot-Schneider, C.; Alonso, F.J. Statistical approach of the influence of petrography in mechanical properties and durability of granitic stones. *Environ. Earth Sci.* **2018**, *77*, 287. [\[CrossRef\]](#)
29. Vázquez, P.; Shushakova, V.; Gómez-Heras, M. Influence of mineralogy on granite decay induced by temperature increase: Experimental observations and stress simulation. *Eng. Geol.* **2015**, *189*, 58–67. [\[CrossRef\]](#)
30. Zhang, W.; Sun, Q.; Zhu, S.; Wang, B. Experimental study on mechanical and porous characteristics of limestone affected by high temperature. *Appl. Therm. Eng.* **2017**, *110*, 356–362. [\[CrossRef\]](#)
31. Zhang, W.; Sun, Q.; Hao, S.; Yang, L. Experimental study of the effect of thermal damage on resistivity and mechanical properties of sandstone. *Acta Geodyn. Geomater.* **2015**, *13*, 185–192. [\[CrossRef\]](#)
32. Zhao, F.; Sun, Q.; Zhang, W. Fractal analysis of pore structure of granite after variable thermal cycles. *Environ. Earth Sci.* **2019**, *78*, 677. [\[CrossRef\]](#)
33. Benavente, D.; Lock, P.; Ángeles García Del Cura, M.; Ordóñez, S. Predicting the Capillary Imbibition of Porous Rocks from Microstructure. *Transp. Porous Media* **2002**, *49*, 59–76. [\[CrossRef\]](#)
34. Thomachot-Schneider, C.; Gommeaux, M.; Fronteau, G. Modifications of the porous network of sandstone accompanying the formation of black varnish. *Environ. Geol.* **2008**, *56*, 571–582. [\[CrossRef\]](#)
35. Vázquez, P.; Alonso, F.J.; Esbert, R.M.; Ordaz, J. Ornamental granites: Relationships between p-waves velocity, water capillary absorption and the crack network. *Constr. Build. Mater.* **2010**, *24*, 2536–2541. [\[CrossRef\]](#)
36. Avdelidis, N.P.; Moropoulou, A.; Marioli Riga, Z.P. The technology of composite patches and their structural reliability inspection using infrared imaging. *Prog. Aerosp. Sci.* **2003**, *39*, 317–328. [\[CrossRef\]](#)
37. Forestieri, G.; de Buergo, M.Á. Infrared Thermography technique (IRT) for the evaluation of the hydric behavior of building stones. *Acta IMEKO* **2018**, *7*, 20–23. [\[CrossRef\]](#)
38. Ludwig, N.; Rosina, E.; Sansonetti, A. Evaluation and monitoring of water diffusion into stone porous materials by means of innovative IR thermography techniques. *Measurement* **2018**, *118*, 348–353. [\[CrossRef\]](#)
39. Zhang, F.; Zhang, X.; Li, Y.; Tao, Z.; Liu, W.; He, M. Quantitative description theory of water migration in rock sites based on infrared radiation temperature. *Eng. Geol.* **2018**, *241*, 64–75. [\[CrossRef\]](#)
40. Grinzato, E.; Marinetti, S.; Bison, P.G.; Concas, M.; Fais, S. Comparison of ultrasonic velocity and IR thermography for the characterisation of stones. *Infrared Phys. Technol.* **2004**, *46*, 63–68. [\[CrossRef\]](#)
41. Mineo, S.; Pappalardo, G. InfraRed Thermography presented as an innovative and non-destructive solution to quantify rock porosity in laboratory. *Int. J. Rock Mech. Min. Sci.* **2019**, *115*, 99–110. [\[CrossRef\]](#)
42. Mineo, S.; Pappalardo, G. The Use of Infrared Thermography for Porosity Assessment of Intact Rock. *Rock Mech. Rock Eng.* **2016**, *49*, 3027–3039. [\[CrossRef\]](#)
43. Thomachot-Schneider, C.; Vázquez, P.; Gommeaux, M.; Lelarge, N.; Conreux, A.; Drothière, X.; Mouhoubi, K.; Bodnar, J.-L. Thermal response of building stones contaminated with salts. *Constr. Build. Mater.* **2019**, *226*, 331–344. [\[CrossRef\]](#)
44. Pappalardo, G.; Mineo, S.; Zampelli, S.P.; Cubito, A.; Calcaterra, D. InfraRed Thermography proposed for the estimation of the Cooling Rate Index in the remote survey of rock masses. *Int. J. Rock Mech. Min. Sci.* **2016**, *83*, 182–196. [\[CrossRef\]](#)
45. Pappalardo, G.; Mineo, S. Investigation on the mechanical attitude of basaltic rocks from Mount Etna through InfraRed Thermography and laboratory tests. *Constr. Build. Mater.* **2017**, *134*, 228–235. [\[CrossRef\]](#)
46. Kim, K.; Kemeny, J.; Nickerson, M. Effect of Rapid Thermal Cooling on Mechanical Rock Properties. *Rock Mech. Rock Eng.* **2014**, *47*, 2005–2019. [\[CrossRef\]](#)
47. Robert, R. Analytical Characterization of Porous Geomaterials: Reference Assessment in Some Sedimentary Rocks. Ph.D. Thesis, Humboldt-Universität zu Berlin, Berlin, Germany, 2004.
48. Vera, J.A. *Geología de España*; SGE-IGME: Madrid, Spain, 2004.
49. Chaki, S.; Takarli, M.; Agbodjan, W.P. Influence of thermal damage on physical properties of a granite rock: Porosity, permeability and ultrasonic wave evolutions. *Constr. Build. Mater.* **2008**, *22*, 1456–1461. [\[CrossRef\]](#)
50. Dwivedi, R.D.; Goel, R.K.; Prasad, V.V.R.; Sinha, A. Thermo-mechanical properties of Indian and other granites. *Int. J. Rock Mech. Min. Sci.* **2008**, *45*, 303–315. [\[CrossRef\]](#)
51. Homand-Etienne, F.; Houpert, R. Thermally induced microcracking in granites: Characterization and analysis. *Int. J. Rock Mech. Min. Sci. Geomech. Abstr.* **1989**, *26*, 125–134. [\[CrossRef\]](#)
52. Reuschlé, T.; Gbaguidi Haore, S.; Darot, M. The effect of heating on the microstructural evolution of La Peyratte granite deduced from acoustic velocity measurements. *Earth Planet. Sci. Lett.* **2006**, *243*, 692–700. [\[CrossRef\]](#)
53. Tang, Z.C.; Sun, M.; Peng, J. Influence of high temperature duration on physical, thermal and mechanical properties of a fine-grained marble. *Appl. Therm. Eng.* **2019**, *156*, 34–50. [\[CrossRef\]](#)
54. Huang, Y.-H.; Yang, S.-Q.; Tian, W.-L.; Zhao, J.; Ma, D.; Zhang, C.-S. Physical and mechanical behavior of granite containing pre-existing holes after high temperature treatment. *Arch. Civ. Mech. Eng.* **2017**, *17*, 912–925. [\[CrossRef\]](#)
55. Kumari, W.G.P.; Ranjith, P.G.; Perera, M.S.A.; Chen, B.K.; Abdulagatov, I.M. Temperature-dependent mechanical behaviour of Australian Strathbogie granite with different cooling treatments. *Eng. Geol.* **2017**, *229*, 31–44. [\[CrossRef\]](#)

56. Li, B.; Ju, F.; Xiao, M.; Ning, P. Mechanical stability of granite as thermal energy storage material: An experimental investigation. *Eng. Fract. Mech.* **2019**, *211*, 61–69. [\[CrossRef\]](#)
57. Ozguven, A.; Ozelik, Y. Investigation of some property changes of natural building stones exposed to fire and high heat. *Constr. Build. Mater.* **2013**, *38*, 813–821. [\[CrossRef\]](#)
58. Thermtest Thermal Conductivity Measurement & Testing Service. Available online: <https://thermtest.com/> (accessed on 7 January 2021).
59. Homand-Etienne, F. *Manuel de Mécanique des Roches*; Presses des MINES: Paris, France, 1986.
60. Freire-Lista, D.M.; Fort, R.; Varas-Muriel, M.J. Thermal stress-induced microcracking in building granite. *Eng. Geol.* **2016**, *206*, 83–93. [\[CrossRef\]](#)
61. Tiskatine, R.; Oaddi, R.; Ait El Cadi, R.; Bazgaou, A.; Bouirden, L.; Aharoune, A.; Ihlal, A. Suitability and characteristics of rocks for sensible heat storage in CSP plants. *Sol. Energy Mater. Sol. Cells* **2017**, *169*, 245–257. [\[CrossRef\]](#)
62. Megawati, M.; Madland, M.V.; Hiorth, A. Mechanical and physical behavior of high-porosity chalks exposed to chemical perturbation. *J. Pet. Sci. Eng.* **2015**, *133*, 313–327. [\[CrossRef\]](#)
63. Nermoen, A.; Korsnes, R.I.; Aursjø, O.; Madland, M.V.; Kjorslevik, T.A.C.; Østensen, G. How Stress and Temperature Conditions Affect Rock-Fluid Chemistry and Mechanical Deformation. *Front. Phys.* **2016**, *4*, 2. [\[CrossRef\]](#)
64. Madland, M.V. *Water Weakening of Chalk: A Mechanistic Study*; University of Stavanger: Stavanger, Norway, 2005.
65. Addis, M.A. The Behaviour and Modelling of Weak Rocks. In Proceedings of the ISRM International Symposium, Pau, France, 30 August–2 September 1989.
66. Brignoli, M.; Santarelli, F.J.; Righetti, C. Capillary phenomena in an impure chalk. In Proceedings of the Rock Mechanics in Petroleum Engineering, Delft, The Netherlands, 29–31 August 1994.
67. Charlez, P.; Heugas, O.; Shao, J.F. *Effect of Temperature on Mechanical Properties of Chalk*; Joint Chalk Research Program: Deauville, France, 1992.
68. DaSilva, F.; Sarda, J.P.; Schroeder, C. Mechanical behavior of chalks. In Proceedings of the North Sea Chalk Symposium, Stavanger, Norway, 1 January 1985.
69. Potts, D.M.; Jones, M.E.; Berget, O.P. *Subsidence above the Ekofisk Oil Reservoirs*; British Maritime Technology: London, UK, 1988.
70. Hellmann, R.; Renders, P.J.; Gratier, J.-P.; Guiguet, R. Experimental pressure solution compaction of chalk in aqueous solutions. Part 1. Deformation behavior and chemistry. Water-rock interactions, ore deposits, and environmental geochemistry: A tribute to David A. Crerar **2002**, *7*, 129–152.
71. Weisbrod, N.; Nativ, R.; Adar, E.M.; Ronen, D.; Ben-Nun, A. Impact of coating and weathering on the properties of chalk fracture surfaces. *J. Geophys. Res. Solid Earth* **2000**, *105*, 27853–27864. [\[CrossRef\]](#)
72. Vasin, R.N.; Nikitin, A.N.; Lokajicek, T.; Rudaev, V. Acoustic emission of quasi-isotropic rock samples initiated by temperature gradients. *Izv. Phys. Solid Earth* **2006**, *42*, 815–823. [\[CrossRef\]](#)
73. Yu, J.; Chen, S.; Chen, X.; Zhang, Y.; Cai, Y. Experimental investigation on mechanical properties and permeability evolution of red sandstone after heat treatments. *J. Zhejiang Univ. Sci. A* **2015**, *16*, 749–759. [\[CrossRef\]](#)
74. Jian-ping, Z.; He-ping, X.; Hong-wei, Z.; Su-ping, P. SEM in situ investigation on thermal cracking behaviour of Pingdingshan sandstone at elevated temperatures. *Geophys. J. Int.* **2010**, *181*, 593–603. [\[CrossRef\]](#)
75. Kim, B.-C.; Chen, J.; Kim, J.-Y. Relation between crack density and acoustic nonlinearity in thermally damaged sandstone. *Int. J. Rock Mech. Min. Sci.* **2020**, *125*, 104171. [\[CrossRef\]](#)
76. Hassanzadegan, A.; Blöcher, G.; Milsch, H.; Urpi, L.; Zimmermann, G. The Effects of Temperature and Pressure on the Porosity Evolution of Flechtinger Sandstone. *Rock Mech. Rock Eng.* **2014**, *47*, 421–434. [\[CrossRef\]](#)
77. Dormieux, L.; Molinari, A.; Kondo, D. Micromechanical approach to the behavior of poroelastic materials. *J. Mech. Phys. Solids* **2002**, *50*, 2203–2231. [\[CrossRef\]](#)
78. Skinner, B.J. Thermal expansion. *Mem. Geol. Soc. Am.* **1966**, *97*, 76–96.
79. Jansen, D.P.; Carlson, S.R.; Young, R.P.; Hutchins, D.A. Ultrasonic imaging and acoustic emission monitoring of thermally induced microcracks in Lac du Bonnet granite. *J. Geophys. Res. Solid Earth* **1993**, *98*, 22231–22243. [\[CrossRef\]](#)
80. Somerton, W.H. *Thermal Properties and Temperature-Related Behavior of Rock/Fluid Systems*; Elsevier Science Ltd.: Amsterdam, The Netherlands; New York, NY, USA, 1992.
81. Gayo, E.; de Frutos, J. Interference filters as an enhancement tool for infrared thermography in humidity studies of building elements. *Infrared Phys. Technol.* **1997**, *38*, 251–258. [\[CrossRef\]](#)
82. Cernuschi, F. Can TBC porosity be estimated by non-destructive infrared techniques? A theoretical and experimental analysis. *Surf. Coat. Technol.* **2015**, *272*, 387–394. [\[CrossRef\]](#)